Effects of high latitude UV radiation on phytoplankton and nekton modelled from field measurements by simple algorithms[1]

Hans C. Eilertsen & Osmund Holm-Hansen

Irradiance measurements from the Barents Sea and coastal areas of northern Norway were used to calibrate a simple-algorithm empirical model that simulate PAR, UVR and UVR inhibition of phytoplankton carbon assimilation. Field measurements showed that UVR levels, in addition to solar zenith angle, were controlled by variations in cloudiness and probably also ozone layer thickness. The relative amount of UV-B and UV-A to PAR increased during periods with heavy cloud cover. Inhibition of phytoplankton photosynthesis, obtained from incubation experiments, was between 50 and 75% close to the surface and was detectable down to ca. 10 m depth. The common spring bloom phytoplankter *Phaeocystis pouchetii* was less sensitive to UVR than centric diatoms. Critical depths (D_{cr}) for increase in phytoplankton biomass modelled from a 40-year time series of meteorological data from Lofoten were shallower during periods with elevated UVR levels, but we suggest that total annual production is not severely affected. Nauplii of the copepod *Calanus finmarchicus* start to feed during the post-spring bloom period, and a delayed or prolonged spring bloom will therefore probably not affect zooplankton or cod (*Gadus morhua*) larvae stocks negatively. Correlation analyses between cod year class strength and modelled UVR levels (r = −0.62) in May indicate a link between years with high UV radiation (clear sky) and poor cod year classes.

H. C. Eilertsen, Norwegian College of Fishery Science, University of Tromsø, N-9037 Tromsø, Norway; O. Holm-Hansen, Polar Research Program, Scripps Institution of Oceanography, University of California at San Diego, La Jolla, CA 92093-0202, USA.

Numerous research programmes have measured ultraviolet radiation and its effects on phytoplankton in southern polar areas (Roy et al. 1989; Helbling, Villafañe, Ferrario et al. 1992; Booth et al. 1994; Neale et al. 1994). There are some reports on atmospheric solar radiation (Hisdal 1986; Henriksen, Claes et al. 1992) and ozone variations in the high Arctic (Henriksen, Larsen et al. 1994), but studies of the spectral composition of visible and UV radiation from northern areas are generally scarce. Information on the submarine light field is nearly totally absent. Calkins & Thordardottir (1980) showed that northern phytoplankton were harmed by UVR, and Helbling, Eilertsen et al. (1996) reported inhibition of photosynthesis down to 10 m, but generally there is a paucity of information on the effects of UVR on marine life in northern areas.

There are several phytoplankton–zooplankton model studies from the area, but these do not include UVR inhibition and consider the net

[1] This paper was originally submitted in connection with the International Symposium on Polar Aspects of Global Change, Tromsø, Norway, 24–28 August 1998. – The Editor.

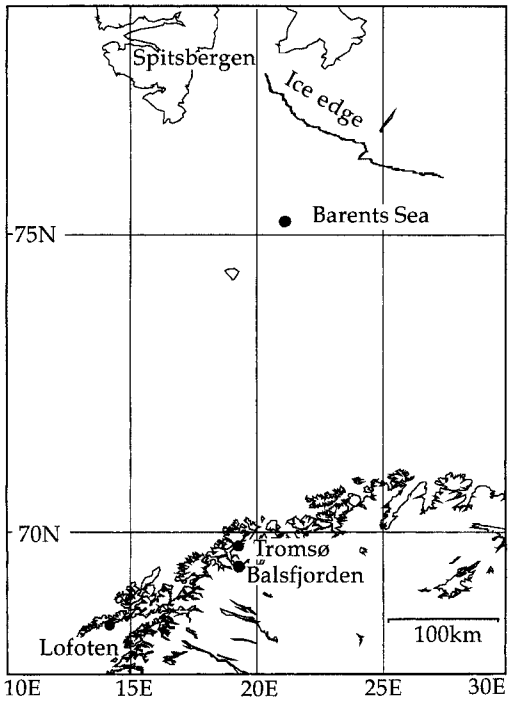

Fig. 1. The sampling stations in the Barents Sea and northern Norway (see also Table 1). The average ice extent in May 1996 is indicated.

"availability" of photosynthetic available radiation (PAR) to be the sole regulator of phytoplankton biomass available to higher trophic levels (Båmstedt et al. 1991; Slagstad & Støle-Hansen 1991; Hansen & Eilertsen 1995). More mathematically complex algorithms that simulate atmospheric and submarine light fields (Sathyendranath & Platt 1988; Stamnes et al. 1988) and biological weighting functions for inhibition of phytoplankton photosynthesis by UVR (Cullen et al. 1992 and references therein) are available. Attempts by us to use these showed that they failed to reproduce the actual observed events. The reason for this, we assume, is simply the previously mentioned lack of knowledge of UVR related physical and biological processes in northern areas. In addition, these models, when coupled to relevant phytoplankton production models need to be run on expensive high quality computers.

The present study, therefore, simply relates UVR to PAR and PAR to phytoplankton photosynthesis based on regressions between the parameters and actual measured data from the area. As a model area we have chosen Lofoten/Vestfjorden, i.e. the main spawning area for north-east Arctic cod (*Gadus morhua*).

Methods

The irradiance and phytoplankton data we used were collected during cruises to the Barents Sea, fiords in northern Norway (Balsfjorden, which is outside Tromsø, and Vestfjorden, in Lofoten) and long-term irradiance series from a ground-based station in Tromsø (Fig. 1, Table 1). Atmospheric and subsurface measurements were performed with a multichannel narrow bandwidth filter instrument (Biospherical Instruments, PUV500/510) with four channels (bandwidth of 10 nm at full width half maximum) centred at 305, 320, 340 and 380 nm. Photosynthetic available radiation (PAR, 400–700 nm) was recorded as quanta. The instrument was calibrated at the factory prior to the measurements in addition to routine calibrations carried out each half year in Tromsø. The total drift of the instrument was at maximum 2.6% per

Table 1. Data used in investigation. I means photosynthesis incubator experiments and S in situ. Irradiance measurements included both PAR and UVR; phytoplankton sampling comprised measurements of photosynthesis (^{14}C method), Chl*a* and species composition and abundance.

Locality sampled	Experimental period	Irradiance logged on surface	Irradiance depth profiles	Phytoplankton sampling/^{14}C	Remarks
Balsfjorden	19.04.95–20.04.95	whole period	4 daily	two daily, I	cruise R/V "Jan Mayen"
Lofoten	10.04.96–13.04.96	whole period	6 daily	one daily, I, S	cruise R/V "Jan Mayen"
Tromsø	01.01.96–13.05.96	1.03.–13.05.96			ground-based
Barents Sea	15.05.96–25.05.96	16.05.–25.05.96	6 daily	one daily, I, S*	cruise R/V "Jan Mayen"
Tromsø	19.09.97–07.11.97	whole period		ground-based	ground-based
Tromsø	28.03.98–15.06.98	whole period		ground-based	ground-based
Lofoten	01.01.57–31.12.96				meteorological data

*In the Barents Sea in 1996, in situ experiments were only performed on 20, 21, 22 and 24 May.

year and the cosine error for the subsurface (PUV-500) instrument was maximum 4%. During the cruises, the atmospheric sensor (PUV-510) was placed 13 m above the sea surface and underwater measurements were done with the sun perpendicular to the side of the boat where measurements were made. The ground-based recording of solar radiation was done with the same sensor placed 20 m from the seashore, 15 m asl on the southern part of Tromsø Island, where shadowing from surrounding mountains was minimal.

Sea water was collected by Niskin and Hydro Bios 5-litre water bottles. Fixed sampling depths were 0, 10, 20, 30 and 50 m. Chlorophyll *a* (extraction four hours, measuring C. V. 3.1%, duplicate samples; results used are means) was measured fluorometrically (Holm-Hansen & Riemann 1978) in a Turner Designs fluorometer. The volumes filtered through GF/F glass fiber filters were adjusted according to the amounts of phytoplankton present and varied between 50 and 500 ml. For analysis of quantitative and qualitative phytoplankton variations, water samples were sedimented immediately after sampling for a minimum of two hours and counted in 2 ml chambers using an inverted microscope.

To determine the effects of UVR on phytoplankton photosynthesis, we used an incubator on the ship's deck and in situ incubations (Table 1). Phytoplankton samples from 0.1 and 10 m depth were placed in 50 ml quartz tubes (horizontally) just below the surface of the tank water. During in situ experiments, 50 ml quartz tubes with phytoplankton were placed at 0.1, 5 and 10 m depths. We used three different radiation treatments in all experiments: a) exposure to UV-B, UV-A and PAR (quartz); b) UVA and PAR (quartz tubes covered with mylar film, 50% transmission at 323 nm); and c) only PAR (tubes covered with Plexiglas UF-3 filters, 50% transmission at 400 nm). Samples were inoculated with 5 μCi (0.185 Mbq) of radiocarbon labelled bicarbonate. All experiments were centred around noon (true local time), generally from 1000 h to 1400 h. In Balsfjorden we performed additional experiments from 1500 h–1800 h (Table 1).

Meteorological observations (cloud cover, 0–8; visibility, km; relative humidity, %) were obtained from the Norwegian Meteorological Institute to be used for Tromsø and Balsfjorden. For Lofoten we used data collected at Skrova, outside Svolvær. Meteorological data were typically collected at 0700 h, 1300 h and 1900 h and occasionally also at 0100 h. During the cruises observations were recorded hourly.

The main spawning area for north-east Arctic cod is Lofoten. After the larvae have hatched in the Lofoten area they drift northwards into the Barents Sea, where they reside most of their lives (Fig. 1). As a measure of variation in cod stock recruitment for the years 1957–1996 we used data from group III (three year old cod) surveys (VPA-Statistics) for the period 1957–1970 (Sætersdal & Loeng 1987) combined with the XSA (eXtended Survivors Analysis). This is in accordance with the standard method suggested by ICES (Thoresen 1998). Data from 1966–1995 were corrected for time trends in trawling efficiency (Nakken & Raknes 1996). To examine possible relationships between UVR and the size of cod stocks, cod stock assessments were normalized using this formula: (measured value for year − mean value for whole period)/mean value for whole period. The strength of each year class is also dependent on the numbers of cod that spawn in Lofoten. Each year's total catch of cod in Lofoten for 1957–1996 was therefore transformed to fractions of the mean (fraction = measured value for year/mean value for period). Finally the normalized stock value for each year was corrected by multiplying with this fraction.

Model description

Basic equations

The basis for the atmospheric radiation model was the algorithm in Frouin et al. (1989), where solar irradiance (I_{PAR}) for clear sky is computed in W m^{-2} after input of surface visibility, humidity and regression coefficients for maritime atmospheres and solar zenith angle:

$$I_{PAR} = I_R * \left(\frac{d}{d_0}\right)^2 * \cos\theta \frac{\exp\left[-\left(a + \frac{b}{V}\right) I\cos\theta\right]}{1 - A\left(a' + \frac{b'}{V}\right)} * \exp\left[-a_\nu \left(\frac{U_\nu}{\cos\theta}\right)^{b_\nu}\right] * \exp\left[-a_0 \left(\frac{U_0}{\cos\theta}\right)^{b_0}\right] \quad (1)$$

I_R is the monochromatic extraterrestrial irradiance

integrated over 400–700 nm (PAR), $\frac{d}{d_0}$ is the ratio of actual to mean Earth-Sun separation, a and b are regression coefficients representing different aerosol types, subscripts v and 0 denote water vapour and ozone, A is albedo, V (km) is surface visibility and U (at-cm) is vertically integrated absorber amount. Coefficients for maritime atmospheres were from Frouin et al. (1989). Solar zenith angle (θ) was computed at given geographical position and time according to the equations in Iqbal (1983). The model was set to integrate over 10 minute intervals.

Calibration of the model using atmospheric (PAR) field data

To calibrate for clear sky conditions, we used meteorological observations made at fixed times (0100 h, 0700 h, 1300 h and 1900 h). Since heavy cloud cover is a characteristic feature of the region, we modelled PAR during shorter periods when cloud cover was zero and where the irradiance plots revealed stable atmospheric conditions. The data sets we used were: Lofoten, 10.04.96 0000 h to 11.04.96 0000 h; Barents Sea, 20.05.96, from 0600 h to 0740 h; Tromsø, 01.10.97, 1300 h to 2100 h and 10.04.98, 0600 h to 2100 h (see Table 1). During initial test simulations, the model underestimated irradiance at all zenith angles, but the linear correlation between measured (μmol quanta $cm^{-2}\,s^{-1}$) and PAR (Wm^{-2}) simulated from the above data sets was r = 0.96 at p = 0.05. Since we at present have no explanations for this other than that cloud cover may be systematically overestimated in the meteorological registrations or that special atmospheric conditions prevailed in these areas, we simply increased the output from the model by a factor of 38% (Fig. 2). The conversion factor to convert PAR measured as μmol quanta $cm^{-2}\,s^{-1}$ to Wm^{-2} (2614.286) was obtained from correlation analysis of the same "clear period" data sets. We thereafter calibrated the model against various degrees of cloud cover by performing linear and non linear correlation analysis on measured PAR vs. cloud cover, visibility and solar zenith angle. The best fit was between irradiance (PAR) and cloud cover (r = 0.78). This is in accordance with the normal assumption that the transmission is a strong function of cloud optical depth and to a much lesser degree of solar zenith angle (Madronich 1993):

$$I_c = I_{PAR}\,(1-(0.0017 + 11.096 * C)/100) \quad (2)$$

where C is cloud cover (1–8) and I_c is cloud corrected PAR. We then proceeded to simulate atmospheric PAR for all the periods when we had both meteorological observations and atmospheric irradiance measurements. The fit for all sampling periods pooled (Fig. 3, Table 1) was a linear correlation coefficient of r = 0.74. Cloud cover and possibly also visibility are measures influenced by the observer. We found no consistent difference between the localities, and equation 2 was therefore used in the further modelling.

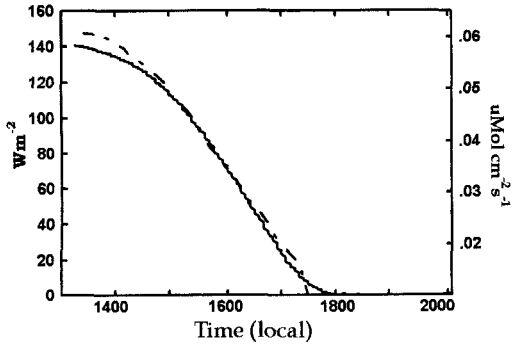

Fig. 2. Measured (dashed line, right y-axis) and modelled (solid line, left y-axis) PAR (400–700 nm) from ground-based station in Tromsø on 1 October 1997 (after calibration of the model).

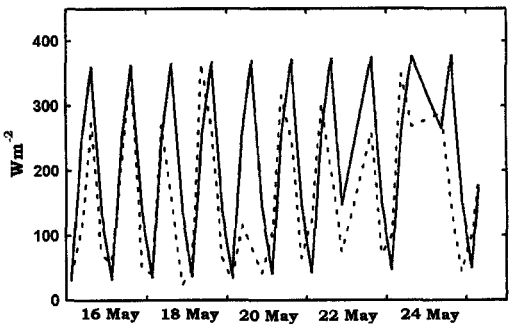

Fig. 3. Measured (dashed line) and modelled (solid line) PAR. Data from the Barents Sea in 1996 (see Table 1).

PAR vs. UVR correlations

Calculated correlations between fractional cloud cover and UVR was non-significant. We therefore inspected ratios between 305, 320 nm and 340, 380 nm and PAR at different cloud covers. These ratios differed statistically significantly (for all

Table 2. Relations used to model UV-B from PAR and UV-A:PAR relations. The algorithms were obtained from linear regression analysis forced through zero (r = 0.65–0.79).

UV-B (305), CC = 8	UV-B = 0.00082*PAR
UV-B (305), CC < 8	UV-B = 0.00058*PAR
UV-A (340), CC = 8	UV-A = 0.14701*PAR
UV-A (340), CC < 8	UV-A = 0.05187*PAR

wavelengths) between cloud cover 8 and the incidences when cloud cover was lower than 8 (0–7). The general picture was that the relative amount of UVR to PAR at "full" cloud cover (8), was greater than at lower cloud covers (0–7). This increased with wavelength (Table 2, Figs. 4, 5). This is in accordance with findings of Hisdal (1986). Diurnal or seasonal effects in the above-mentioned ratios were absent, similar to findings of Gautier et al. (1994) from Antarctica. In the further modelling of atmospheric UVR we chose to use only the 305 nm: PAR ratios (Table 2) in the further modelling. As we will show later, this was partially justified by, the fact that the deleterious effects that UV-B and UV-A had on phytoplankton photosynthesis were quantitatively similar.

Subsurface irradiance

It is difficult to achieve good readings with the sensor submerged immediately under the surface due to scattering effects. We therefore used measurements from 0.15 m depth and "back-calculated" this to 0 m depth from k values from corresponding 0.15 and 0.5 m irradiances (for each wavelength). From these 0 m subsurface PAR values and PAR incident upon the surface, relations were examined between albedo (A,

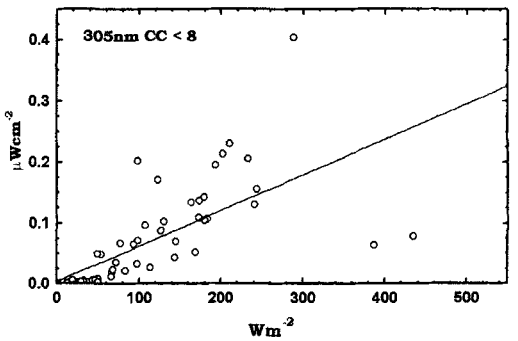

Fig. 4. The relation between PAR (x-axis) and UVR-305 nm (y-axis) in the data from Table 1 when cloud cover was less than 8 (r = 0.78).

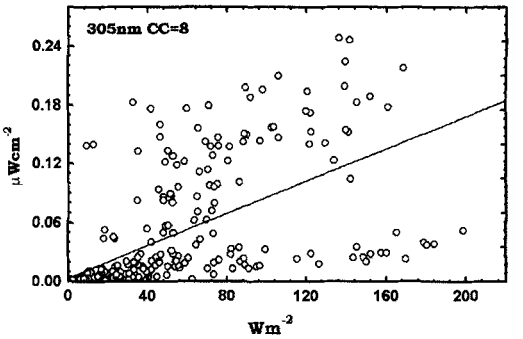

Fig. 5. The relation between PAR (x-axis) and UVR-305 nm (y-axis) in the data from Table 1 when cloud cover was 8 (r = 0.72). Note difference in scale on Y-axis relative to Fig. 4.

amount of reflected light at surface), solar zenith angle (θ), cloud-cover and sea-roughness (here expressed as linearly correlated to wind stress). The wind equation we used was (Gill 1982):

$$\tau = C_D \rho v^2 \quad (3)$$

where τ is wind stress, ρ is the air pressure and v is the wind speed. The Drag coefficient is $C_D = 1.1 \times 10^{-3}$ for $v < 6\ \mathrm{m\ s^{-1}}$, and $10^3 \times C_D = 0.61 + 0.063$ for $6\ \mathrm{m\ s^{-1}} < v < 22\ \mathrm{m\ s^{-1}}$.

By using multiple regression analysis we found a significant correlation only between albedo and solar zenith angle. At low wind speeds and $\theta < 40°$ specular reflectance is mainly dependent on the angle of the sun (Gregg & Carder 1990). By further analysing the data, using a non-linear fitting procedure, the best relationship between albedo and θ was found:

$$\mathrm{log10}\ (albedo) = (cos\theta - 0.273)/-0.113 \quad (4)$$

where θ is angle in degrees times Pi/180.

The diffuse attenuation coefficient used to calculate subsurface PAR, was obtained by analysing Chl$a$ and subsurface PAR data sets (Table 1):

$$k = (\mathrm{Chl}a + 0.589)/11.787 \quad (5)$$

At zero chlorophyll this function yields a k of ca. 0.05 (r = 0.75), indicating that some dissolved organic material (yellow substance) was present.

To obtain an algorithm for UVR attenuation, we statistically examined the relations between subsurface UVR and solar zenith angle, cloud cover, visibility, Chl$a$ and computed k values for the UVR wavelengths. The best correlations were between UVR and Chl$a$, and we obtained the

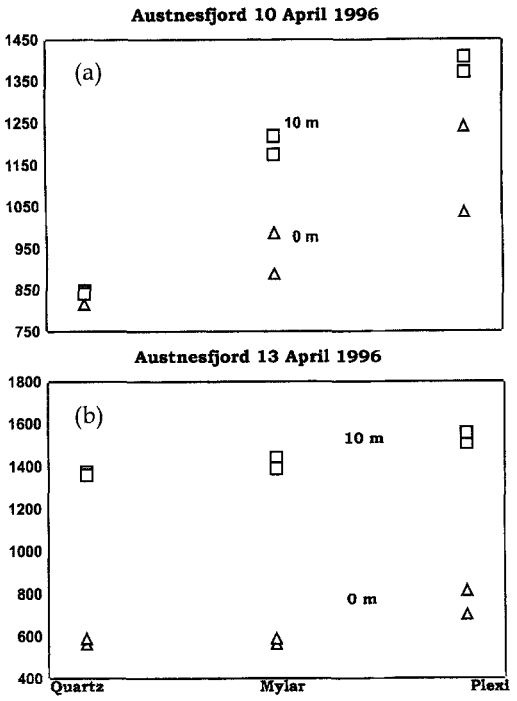

Fig. 6. Incubator experiments performed in Austnesfjorden in Lofoten 1996. Y-axis is relative photosynthesis in dpm*10 (a) on a clear day, mean cloud cover ca. 1; and (b) on a day with mean cloud cover ca. 6.

following linear relations describing the attenuation for UVR (r = 0.69, 0.72):

$$k\text{-}305\ \text{nm} = 0.52193 + 0.02885*\text{Chl}a\ \text{l}^{-1} \quad (6)$$

Carbon assimilation calculations

To calculate carbon assimilation (P, mg C m^{-3}) we used the equation in Webb et al. (1974):

$$= \left(\frac{Chl}{C}\right) P^B (1 - e^{-\alpha Q_{s(p)}/P^B}) \quad (7)$$

where P^B is the maximum photosynthetic rate [mg C mg Chla^{-1} h^{-1}], α is the photosynthetic efficiency [mg C mg Chla^{-1} h^{-1} W m^{-2}], and $Q_{s(p)}$ ($= I_{PAR}$) is PAR [W m^{-2}] at depth z. Photosynthetic coefficients were from Båmstedt et al. (1991) and Hansen & Eilertsen (1995): $P^B = 2.5$; $\alpha = 0.15$; Chl:C = 0.015. During modelling of critical depth a constant loss rate (respiration, sinking, grazing) of 6% was assigned to phytoplankton biomass at any depth at any time. Variation in "critical depth" (Sverdrup 1953) was then computed by ordering the model to calculate photosynthesis (P) and accumulated loss rate modelled in one hour intervals, for each 24 hour period downwards over one metre intervals. Employing iteration techniques, a programme then found the depth where total photosynthesis was equal to total loss (D_{cr} = "critical depth").

UVR inhibition of photosynthesis

The incubator experiments showed, similar to the results reported by Helbling, Eilertsen et al. (1996), that UV-B and UV-A each accounted for about 50% of total inhibition of carbon assimilation (Fig. 6). The highest degree of inhibition at Lofoten in 1996 (Fig. 6) was considerably lower than in Helbling, Eilertsen et al. (1996), even though the levels of UV-A and UV-B were comparable. Phytoplankton species were typical for the area (Eilertsen et al. 1981), i.e. mainly centric diatoms and *Phaeocystis pouchetii* (Table 3). The highest degree of inhibition we found at Lofoten in 1996 (Fig. 6) was considerably lower than in Helbling, Eilertsen et al. (1996), even though the UVR levels were comparable. The composition of the phytoplankton stocks in our investigation, typical of spring blooms in the area (Føyn 1929; Eilertsen et al. 1981), was mainly centric diatoms of the genus *Chaetoceros* and haptophycean *Phaeocystis pouchetii* (Table 3). In the Helbling, Eilertsen et al. (1996) investigation, a larger part of the phytoplankton was solitary

Table 3. Species composition and mixed depth during the incubator and in situ experiments. All the mixed depths (during mid-April) are means between the samplings, and all the observed pycnoclines were "weak", i.e. $d\sigma_t \approx 0.2$–0.5.

Locality	Period	Main species	Mixed depth
Balsfjorden	19.04.95–20.04.95	*Chaetoceros socialis, Phaeocystis pouchetii*	22 m
Lofoten	10.04.96–13.04.96	*Chaetoceros socialis*, 50% resting spores	18 m
Barents Sea	15.05.96–25.05.96	*Phaeocystis pouchetii, Thalassiosira nordenskioeldii, Chaetoceros* sp.	120 m

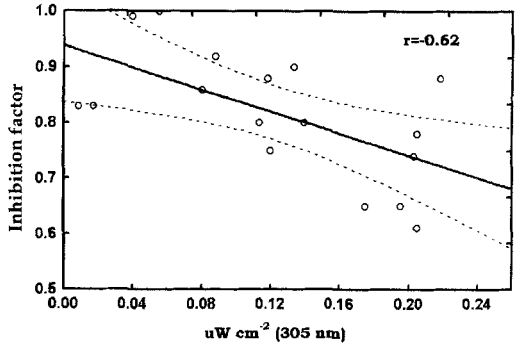

Fig. 7. Linear regression of relative inhibition of phytoplankton carbon assimilation (1 = no inhibition, 0 = full inhibition) vs. UV-B (305 nm). Species composition is in Table 3. Dashed line is 95% confidence level.

flagellates, and this may be the reason why results were different.

The results from the in situ experiments from 0 and 5 m corresponded with the incubator experiments and since the 10 m in situ experiments showed only 5–9% more sensitivity to UVR, we pooled all the measurements (Fig. 7). For convenience, we neglected the slight curvilinear shape of the inhibition, and used the relation below between radiation at 305 nm and "inhibition" to model total UVR (UV-B + UV-A) inhibition during the model runs, i.e. the potential gross production modelled from equation 7 was multiplied with a inhibition factor (F) to achieve UVR inhibited production:

$$F\ (1-0) = 0.93915 - 0.9907 * \text{nm } 305 \quad (8)$$

This relation is not forced through zero, and in the model F was assigned a value of 1.0 (no inhibition) when subsurface radiation at 305 nm was modelled to zero.

Finally we modelled critical depth for 40 in Lofoten, using equations 1 and 2 to model atmospheric PAR, 4 and 5 to model underwater PAR, 6 to model underwater UVR (305 nm) and 7 and 8 to model production with and without inhibition.

Discussion

At the time of the onset of the spring bloom, late in March, daily UVR doses were normally low (Fig. 8), similar to observations for the same period in

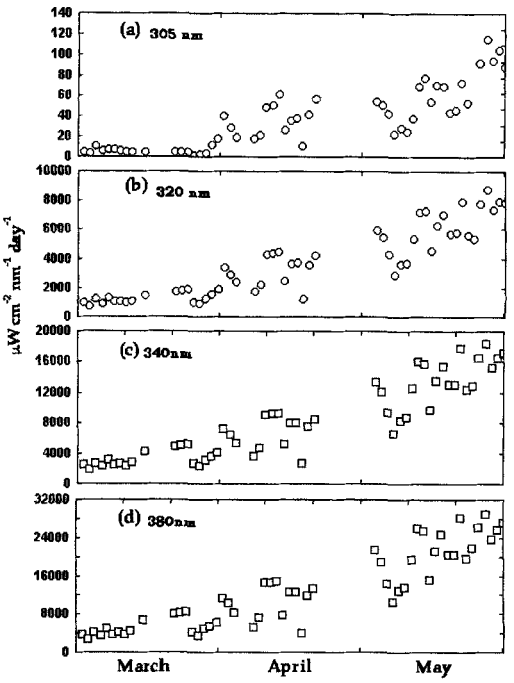

Fig. 8. General variations in daily doses of UV radiation at (a) 305 and (b) 320 nm (circles), and at (c) 340 and (d) 380 nm (squares). Logged at ground-based station in Tromsø during the spring of 1996.

Antarctica (Helbling, Villafañe & Holm-Hansen 1994). Mean daily 305 nm values during mid-May were around 0.0025 µW cm^{-2} nm^{-1} and peak values during mid day were 0.4–0.5 µW cm^{-2} nm^{-1}. The increase in daily doses that can be observed in Fig. 8 is more a function of increased day length than maximum levels observed around noon. This is lower than earlier observed in July in Tromsø (Helbling, Villafañe & Holm-Hansen 1994), and considerably lower than the highest values observed in the southern ocean (Helbling, Chalker et al. 1996). The radiation climate in Tromsø is also highly variable due to frequent periods with heavy cloud cover. Even though day length increases rapidly at this time of the year, UVR levels in May may occasionally be lower than during late March (Fig. 8). The faster increase in UV-B relative to UV-A in May can probably be attributed to a thinning of the ozone layer due to extensive cold air outbreaks in the upper stratosphere layers (NILU 1996).

When modelling phytoplankton critical depth for 40 years in Lofoten, with and without UVR inhibition, we observed the most extensive shal-

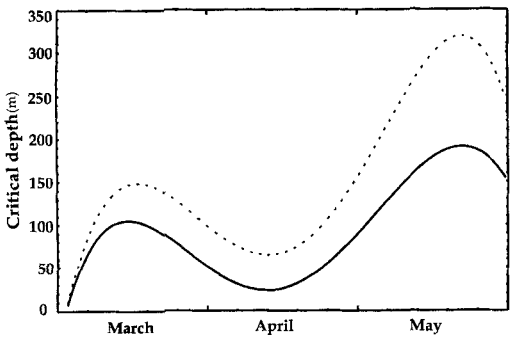

Fig. 9. Modelled critical depth with (solid line) and without (dashed line) UVR inhibition of phytoplankton growth. When modelling, phytoplankton biomass (Chl*a*) was assumed to be distributed uniformly with depth. Biomass distribution vs. time was constructed from data collected during several cruises to Lofoten (unpubl. data), i.e. nearly "clear" water 15 March (0.05 μg Chla l^{-1}), peak of 14 μg Chla l^{-1} 13 April, declining values to 2.6 μg Chla l^{-1} at the end of May. Bulge in April is peak of spring bloom = high k values.

lowing of D_{cr}, in May, i.e. after the culmination of the spring bloom (Figs. 9, 10). During early spring the critical depths are shallow in the area due to short days and low solar zenith angles (Fig. 10). Inhibition of photosynthesis was not so pronounced during early spring, but mixed depths may at this time of year extend to the bottom (Hansen & Eilertsen 1995; Hegseth et al. 1995), and this may cause delayed or slowed spring bloom during years with clear sky. During other years (with heavy cloud cover) little or no discernible effect of UVR inhibition can be expected. According to our model runs, on 8423 out of 13354 days (63%) the growth of phytoplankton (photosynthesis) was reduced by 0 to 10% by UVR, while on 4804 of 13354 days (37%) there was no UVR inhibition (Fig. 10).

As to the further progress of the blooms during the years when the sky is at its clearest, we assume that inhibition in the upper water layers results in retardation of total growth, and possibly a larger part of growth takes place at greater depths. This must also to some degree be compensated for by lowered k values in the upper layers. Also, since the mixed depths are deep and the pycnoclines are weak (Table 3), some additional (new) plant nutrients will be available within the euphotic zone. The net effect of this will be slightly delayed blooms with different vertical distributions of phytoplankton biomass, as can often be observed during late spring bloom and early summer phases in the north (Eilertsen et al. 1981).

In regard to the consequences of this for species at higher trophic levels, for example *Calanus finmarchicus* on which cod larvae in the area feed, we believe no negative effects of a slightly delayed bloom should be expected. This is because the nearshore/coastal stocks of this copepod spawn during late bloom phases, and consequently the nauplii of this species feed on remains of the spring bloom.

We have earlier observed during UVR experiments in Lofoten that 2–4 week old cod larvae, exposed to high (clear sky) values of UV-B, died after approximately 40 hours. Similar experiments with cod eggs resulted in a lower mortality, but applied TT dimer methods showed relatively high levels of DNA damage (unpubl. data). It has been confirmed by Béland et al. (1999) that clear sky UVR levels may cause mortality in both larvae and eggs of Atlantic cod. Since eggs and early juveniles of cod are present in large densities in the uppermost water layers in Lofoten during late March to May, Sundby et al. (1989) concluded that year class strength of cod is mainly determined at egg and larval stages, and that the exact reasons causing variations in cod year class strength was unknown to them. It is therefore highly possible that year class strength may be influenced by UVR and this is worth investigating. When we correlated the bulk of cod year class data vs. the mean 305 nm radiance level for May in Lofoten for the period 1957–1996, we observed a linear correlation between the selected parameters ($r = -0.51$). Since these analyses are based on data from group III cod surveys, the feeding and survival conditions after the larvae leave Lofoten must influence these figures. It is known that during warm years, feeding conditions in the Atlantic Barents Sea are

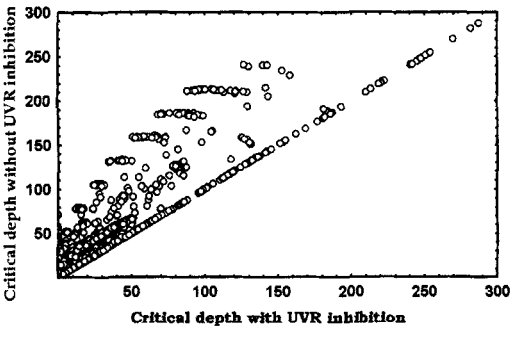

Fig. 10. Correlation plot of critical depth with and without UVR inhibition (Lofoten simulations) for each of the 40 years modelled.

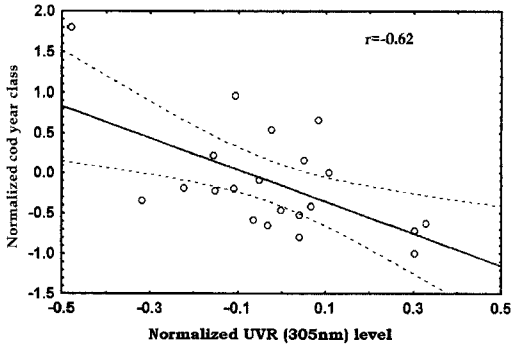

Fig. 11. Linear correlation plot between normalized cod year class and mean level of radiation at 305 nm (for the hours the sun was up) for the month of May.

better than during cold years, and that cold years are much more frequent than warm years (Sætersdal & Loeng 1987). A closer examination of our initial analysis revealed that most of the years that deviated from the line representing the best fit between UV-A in May and year class strength were warm years. When we then re-analysed the data sets and excluded these warm years, we observed a better fit ($r = -0.62$), indicating that there may be a connection between cod year class strength and UVR, at least during cold years (Fig. 11). We are aware that this conclusion may be debated, but it is in our opinion important to investigate this further, with field surveys as well as laboratory experiments involving both UVR and cod eggs and larvae.

References

Båmstedt, U., Eilertsen, H. C., Tande, K. S., Slagstad, D. & Skjoldal, H. R. 1991: Copepod grazing and its potential impact on the phytoplankton development in the Barents Sea. *Polar Res. 10(2)*, 339–353.

Béland, F., Browman, H. I., Alonso Rodriguez, C. & St-Pierre, J.-F. 1999: Effect of solar ultraviolet radiation (280–400 nm) on the eggs and larvae of Atlantic cod (*Gadus morhua*). *Can. J. Fish. Aquat. Sci. 56*, 1–10.

Booth, C. R., Lucas, T. B., Morrow, J. H., Weiler, C. S. & Penhale, P. A. 1994: The United States National Science Foundation's polar network for monitoring ultraviolet radiation. In C. S. Weiler & P. A. Penhale (eds.): *Ultraviolet radiation in Antarctica: measurements and biological effects. Antarct. Res. Ser. 62.* Pp. 17–37. Washington, D.C.: American Geophysical Union.

Calkins, J. & Thordardottir, T. 1980: The ecological significance of solar UV radiation on aquatic organisms. *Nature 283*, 563–566.

Cullen, J. J., Neale, P. J. & Lesser, M. P. 1992: Biological weighing function for the inhibition of phytoplankton photosynthesis by ultraviolet radiation. *Science 258*, 646–650.

Eilertsen, H. C., Schei, B. & Taasen, J. P. 1981: Investigations on the plankton community of Balsfjorden, north Norway. The phytoplankton 1976–1978. Abundance, species composition, and succession. *Sarsia 66*, 121–141.

Frouin, R., Ligner, D. W, Gautier, C., Baker, K. S. & Smith, R. C. 1989: A simple analytical formula to compute clear sky total and photosynthetically active solar irradiance at the ocean surface. *J. Geophys. Res. 94(C7)*, 9731–9742.

Gautier, C., He, G., Yang, S. & Lubin, D. 1994: Role of clouds and ozone on spectral ultraviolet-b radiation and biologically active UV dose over Antarctica. In C. S. Weiler & P. A. Penhale (eds.): *Ultraviolet radiation in Antarctica: measurements and biological effects. Antarct. Res. Ser. 62.* Pp. 83–92. Washington, D.C.: American Geophysical Union.

Gill, A. E. 1982: *Atmosphere–ocean dynamics.* London: Academic Press.

Gregg, W. W. & Carder, K. L. 1990: A simple spectral solar irradiance model for cloudless maritime atmospheres. *Limnol. Oceanogr. 35*, 1657–1675.

Hansen, G. A. & Eilertsen, H. C. 1995: Modelling the onset of phytoplankton blooms: a new approach. In H. R. Skjoldal et al. (eds.): *Ecology of fjords and coastal waters: proceedings of the Mare Nor Symposium on the Ecology of Fjords and Coastal Waters, Tromsø, Norway, 5–9 December, 1994.* Pp. 73–83. Amsterdam: Elsevier.

Hegseth, E. N., Svendsen, H. & Hellum C. 1995: Phytoplankton in fjords and coastal waters of northern Norway: environmental conditions and dynamics of the spring bloom. Pp. 45–72. In H. R. Skjoldal et al. (eds.): *Ecology of fjords and coastal waters: proceedings of the Mare Nor Symposium on the Ecology of Fjords and Coastal Waters, Tromsø, Norway, 5–9 December, 1994.* Pp. 45–72. Amsterdam: Elsevier.

Helbling, E. W., Chalker, B. E., Dunlap, W. C., Holm-Hansen, O. H. & Villafañe, V. E. 1996: Photoacclimation of Antarctic marine diatoms to solar ultraviolet radiation. *J. Exp. Mar. Biol. Ecol., 204*, 85–101.

Helbling, E. W., Eilertsen, H. C., Villafañe, V. E. & Holm-Hansen, O. 1996: Effects of UV radiation on post-bloom phytoplankton populations in Kvalsund, north Norway. *J. Photochem. Photobiol. 33*, 255–259.

Helbling, E. W., Villafañe, V., Ferrario, M. & Holm-Hansen, O. 1992: Impact of natural ultraviolet radiation on rates of photosynthesis and on specific marine phytoplankton species. *Mar. Ecol. Prog. Ser. 80*, 89–100.

Helbling, E. W., Villafañe, V. & Holm-Hansen, O. 1994: Effects of ultraviolet radiation on Antarctic marine phytoplankton photosynthesis with particular attention to the influence of mixing. In C. S. Weiler & P. A. Penhale (eds.): *Ultraviolet radiation in Antarctica: measurements and biological effects. Antarct. Res. Ser. 62.* Pp. 207–227. Washington, D.C.: American Geophysical Union.

Henriksen, K., Claes, S., Svenø, T. & Stamnes, K. 1992: Spectral and visible irradiance measurements in the Barents Sea and Svalbard. *J. Atmos. Terr. Phys. 54*, 1119–1127.

Henriksen, K., Larsen, S. H. H., Shumilov, I. O. & Thorkelsson, B. 1994: Ozone variations in the Scandinavian sector of the Arctic during the AASE campaign and 1989. *Geophys. Res. Lett. 21*, 1775–1778.

Hisdal, V. 1986: Spectral distribution of global and diffuse solar radiation in Ny-Ålesund, Spitsbergen. *Polar Res. 5(1)*, 1–27.

Holm-Hansen, O. & Riemann, B. 1978: Chlorophyll a

determination: improvements in methodology. *Oikos 30*, 438–447.

Iqbal, M. 1983: *An introduction to solar radiation*. Toronto: Academic Press.

Karentz, D. 1994: Ultraviolet tolerance mechanisms in Antarctic marine organisms. In C. S. Weiler & P. A. Penhale (eds.): *Ultraviolet radiation in Antarctica: measurements and biological effects. Antarct. Res. Ser. 62*. Pp. 93–110. Washington, D.C.: American Geophysical Union.

Madronich, S. 1993: The atmosphere and UV-B radiation at ground level. In R. Young et al. (eds.): *Environmental UV photobiology*. Pp. 1–39. New York: Plenum Press.

Nakken, O. & Raknes, A. 1996: Korreksjon av tallrikhetsindekser for 0-gruppe fisk i Barentshavet. (Correction to abundance estimates for 0 group fish in the Barents Sea.) *Fisken og Havet 20*, 1–10.

Neale, P. J., Lesser, M. P. & Cullen, J. J. 1994: Effects of ultraviolet radiation on the photosynthesis of phytoplankton in the vicinity of McMurdo Station, Antarctica. In C. S. Weiler & P. A. Penhale (eds.): *Ultraviolet radiation in Antarctica: measurements and biological effects. Antarct. Res. Ser. 62*. Pp. 125–142. Washington, D.C.: American Geophysical Union.

NILU 1996: *Overvåkning av ozonlaget. (Variations in ozone layer thickness.) NILU Årsrapp. 1996, 696/97, TA-1448/1997*. Norsk Institutt for Luftforskning (Norwegian Institute for Air Research).

Platt, T., Bird, D. & Sathyendranath, S. 1991: Critical depth and marine primary production. *Proc. R. Soc. Lond. B. 246*, 205–217.

Roy, C. R., Gies, P. & Elliott, G. 1989: The A. R. L. solar ultraviolet radiation measurement programme. In W. Refshauge (ed.): *Transactions of the Menzies Foundation, vol. 15*. Pp. 71–76. Melbourne.

Sætersdal, G. & Loeng, H. 1987: Ecological adaption of reproduction in northeast Arctic cod. *Fish. Res. 5*, 253–270.

Sathyendranath, S. & Platt, T. 1988: The spectral irradiance field at the surface and in the interior of the ocean: a model for applications in oceanography and remote sensing. *J. Geophys. Res. 93(C8)*, 9270–9280.

Slagstad, D. & Støle Hansen, K. 1991: Dynamics of phytoplankton growth in the Barents Sea: model studies. *Polar Res. 10(1)*, 173–187.

Stamnes, K., Tsay, S.-C., Wiscombe, W. & Jayaweera, K. 1988: Numerically stable algorithm for discrete-ordinate-method radiative transfer in multiple scattering and emitting layered media. *Appl. Opt. 27*, 2502–2508.

Sundby, S., Bjørke, H., Soldal, A. V. & Olsen, S. 1989: Mortality rates during the early life stages and year-class strength of northeast Arctic cod (*Gadus morhua* L.). *Rapp. P. -v. Réun. Cons. Int. Explor. Mer. 191*, 351–358.

Sverdrup, H. U. 1953: On conditions for the vernal blooming of phytoplankton. *J. Cons. Perm. Int. Explor. Mer. 18*, 287–295.

Thoresen, R. 1998: *Havets ressurser 1998. (The ocean's resources 1998.) Fisken og Havet spec. issue 1*.

Vernet, M., Brody, E. A., Holm-Hansen, O. & Mitchell, G. 1994: The response of Antarctic phytoplankton to ultraviolet radiation: absorption, photosynthesis, and taxonomic composition. In C. S. Weiler & P. A. Penhale (eds.): *Ultraviolet radiation in Antarctica: measurements and biological effects. Antarct. Res. Ser. 62*. Pp. 143–158. Washington, D.C.: American Geophysical Union.

Webb, W. L., Newton, M. & Starr, D. 1974: Carbon dioxide exchange of *Alnus rubra*: a mathematical model. *Oecologia 17*, 281–291.